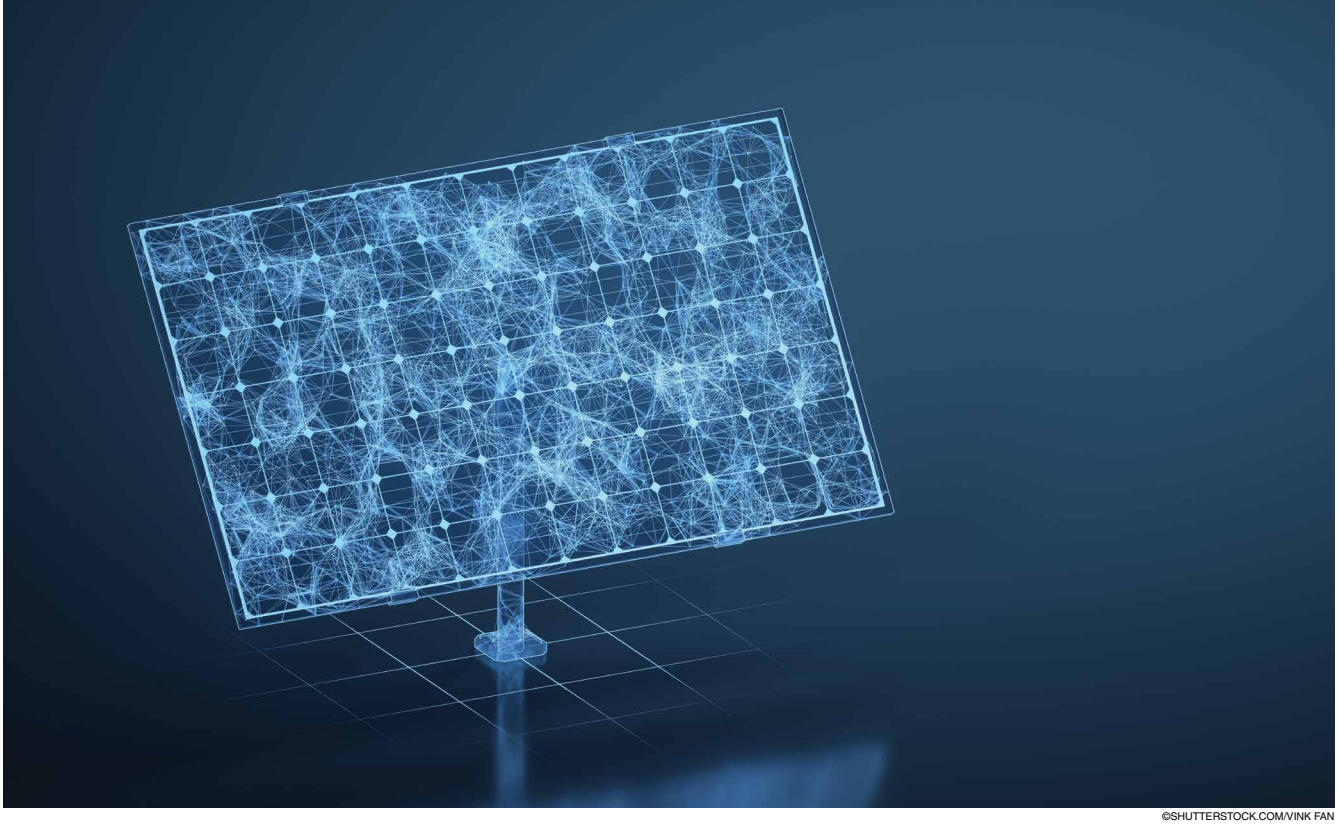

©SHUTTERSTOCK.COM/VINK FAN

Learning-by-Doing: Design and Implementation of a Solar Array Simulator With a SYNDEM Smart Grid Research and Educational Kit

by Kevin Norman, Beibei Ren, and Qing-Chang Zhong

Digital Object Identifier 10.1109/MPEL.2024.3352209
Date of publication: 9 February 2024

Introduction

Topics in control and power electronics play a pivotal role in the transition of power systems from centralized generation to distributed generation, the electrification of transportation, and the improvement of the lives of billions in developing countries. Numerous active sources, such as wind farms, solar farms, distributed energy resources, electric vehicles, energy storage systems, and flexible loads, are being integrated into power systems through power electronic converters [1]. These demand for skilled power electronics and control engineers with a robust foundation in theoretical knowledge, complemented with extensive practical experiences, to effectively navigate emerging and rapidly evolving technologies in the realm of renewable energy. Therefore, enhancing learning effectiveness in these fields is critical for students to bridge the gap between theoretical knowledge and industrial settings. The concept of learning-by-doing emerged in recent decades is a compelling approach that can significantly improve engineering education, particularly, in the context of power electronics and control. It is a dynamic method in which students investigate real-world problems and challenges, fostering not only a deeper understanding of the subject matter but also increasing their engagement levels and critical thinking [2]. Additional advantages include fostering active, self-motivated student engagement in the learning process and empowering them to address doubts independently. This approach may lead to a more effective learning experience than relying solely on a teacher, as students gain heightened awareness of specific challenges through firsthand experiences in solving real-world problems and make new contributions in the field [3].

This approach may lead to a more effective learning experience than relying solely on a teacher, as students gain heightened awareness of specific challenges through firsthand experiences in solving real-world problems and make new contributions in the field [3].

In this article, an attempt to train graduate students through learning-by-doing is reported, through the design and implementation of a solar array simulator (SAS). Simulators, which function as nonlinear power supplies that accurately replicate the current-voltage (I-V) and power-voltage (P-V) characteristics of photovoltaic (PV) modules, are valuable tools to meet the challenges in testing PV systems, such as the need for reproducible test conditions, dependence on atmospheric factors, limited adaptability to different panel configurations, and difficulties in altering irradiance levels [4]. This enables consistent, repeatable testing in an indoor setting, significantly reducing the time and space required for research. This tool provides consistency and time independence, allowing for pre-installation analysis and evaluation in a laboratory environment without the need for large outdoor spaces [5], [6]. As a power electronic system, the design and implementation of a SAS serves as a perfect project for students to learn control and power electronics.

Designing a SAS requires three critical features:

1) Accurate replication of I-V and P-V curves with user-selectable PV panels and connections.
2) Seamless load interfacing.
3) Dynamic operating point adjustment in response to changes in load, irradiance, and temperature [6].

This article details the design and implementation of a SAS using the SYNDEM Smart Grid Research and Educational Kit [1] (hereafter referred to as "the Kit"), a reconfigurable power electronics converter that simplifies system modifications in both electrical and control designs. It allows direct code downloading from MATLAB/Simulink, streamlining the shift from simulation to experimental studies. Its reconfigurable power board supports over 10+ configurations, including various dc–dc and ac–dc converters, both in islanded and grid-connected modes, enhancing user experimentation through simple jumper wire connections.

The work involves configuring both the power and control boards of the Kit, designing the controllers, and implementing the associated codes. The power board is set as a closed-loop rectifier using the θ-converter topology [11], cascaded with a dc–dc buck converter, and provides a common negative dc and neutral ac terminal. The control board integrates the PV model and control algorithms into the digital signal processor (DSP) of the Kit, with an RS485 communication interface tailored for a human machine interface (HMI) in MATLAB/Simulink. Experimental results across various configurations are presented.

Overview of a Solar Array Simulator

A SAS consists of four main components: the PV model, controller, power conversion stage (PCS), and the HMI, as shown in Figure 1. Additionally, the SAS can be linked to a load which can be resistive, inductive, or capacitive in nature or other switched mode power supplies (SMPS) like maximum power point tracking (MPPT) converters, inverters for grid tied applications, and batteries for energy storage [7]. These components play a crucial role and have the following functions [5]:

- PV Model: Generates the I-V characteristic curves of PV modules, which are essential for the closed-loop PCS to replicate PV string properties. The system's accuracy in emulating a real PV module largely relies on the model's performance as it sets the operating point. These I-V curves can be approximated using either analog methods, involving actual PV cells and analog circuits, or digital methods using DSPs, microcontrollers, and FPGAs, which provide more flexibility, particularly for real-time adjustments in temperature and irradiance. In this SAS, a single-diode model with direct calculation is employed, meeting the trade-off between computational efficiency and model accuracy.
- Controller: Monitors and adjusts the PCS output to align with the PV model reference signal. An effective controller is characterized by stable output, rapid response, efficient processing, adaptability to various PV modules, and independence from the converter and load. The direct referencing method (DRM) [5] is often preferred for its simplicity, adjusting the simulator's output to match the desired I-V curve point. In this SAS, a DRM operating in current mode control (CMC) is selected for its quick transient response and high stability [8].
- Power Conversion Stage: Converts the I-V characteristic signal into a power-transmitting signal, tracking the controller's reference signal based on the PV model. This stage is crucial for the SAS' power efficiency and dynamic response. The PCS can utilize linear regulators or SMPS and, in this design, a rectifier coupled with a dc–dc buck converter is selected, because of its simplicity, robustness, and flexibility in testing various model configurations.
- HMI: Acts as the user interface for real-time control and data monitoring. It allows users to set SAS operating conditions, like temperature, solar irradiance, PV panel brand and configurations. For this simulator, RS485 serial communication is used along with MATLAB/Simulink as the front-end software.

Design and Implementation of the SAS

As shown in Figure 2(a), the SAS system comprises of a power board in the Kit that houses the PCS, and a control board that implements the embedded PV model and controllers. An HMI is developed for user-defined control on parameters, such as temperature T, irradiance G, and

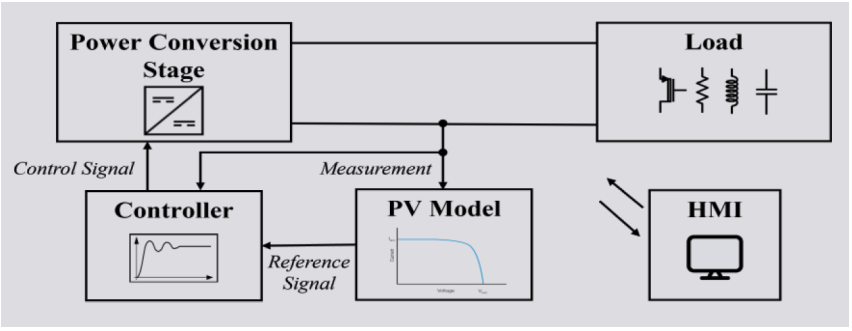

FIG 1 SAS components.

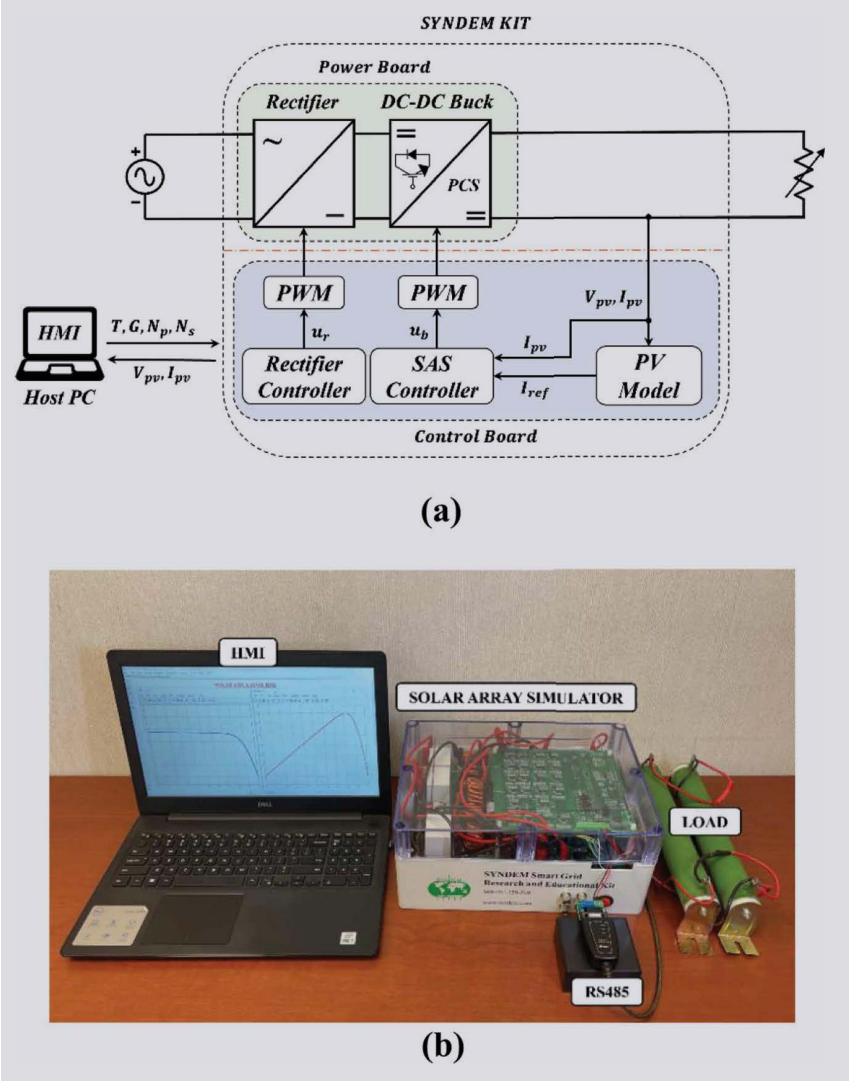

FIG 2 SAS system. (a) System structure. (b) Experimental setup.

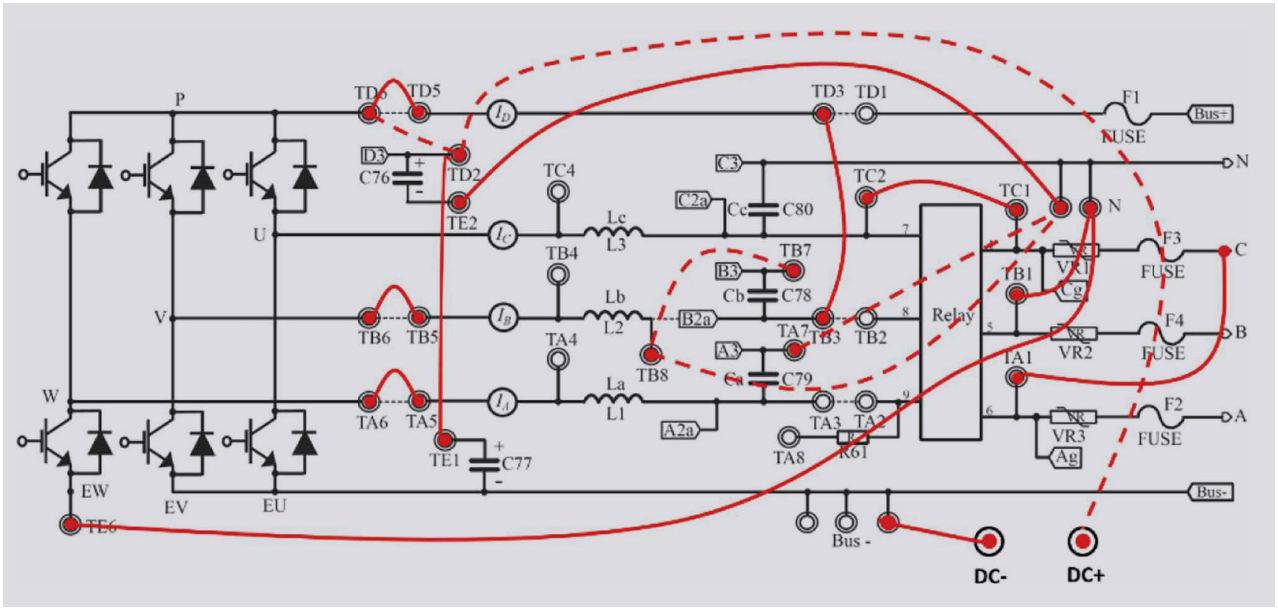

FIG 3 SYNDEM kit main power circuit with SAS connections.

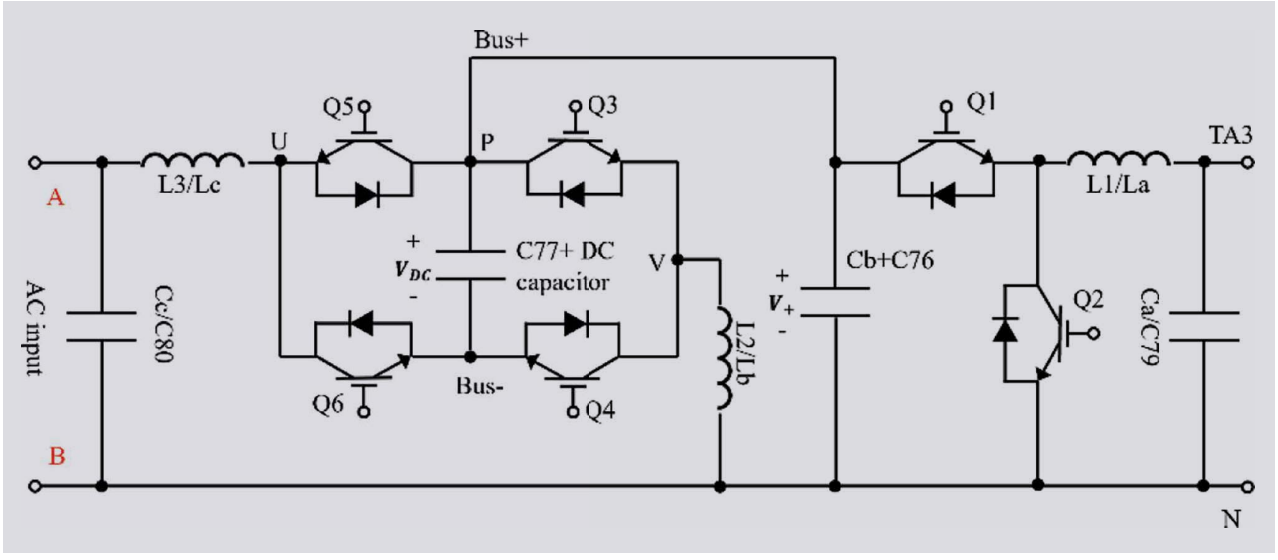

FIG 4 SAS topology—rectifier cascaded with buck converter.

number of panels connected in parallel N_p and series N_s. Figure 2(b) shows the setup.

A. Design of the Power Stage

This work leverages the benefits of the Kit, which includes a Texas Instruments C2000 Control CARD. This component enables automatic code generation from MATLAB/Simulink and TI Code Composer Studio, allowing users to engage with Simulink's graphical programming environment and apply pre-verified control algorithms from simulations. Additionally, the Kit is equipped with a power board that houses various components like IGBTs, relay, current and voltage sensors, inductors, capacitors, and fuses, which would otherwise take months for a skilled person to assemble. Hence, the Kit streamlines the experimental process by eliminating the need to start from scratch in topology design and testing, while its reconfigurability feature simplifies system modifications and controller implementation, assisting researchers in efficiently addressing component modification challenges [1]. Figure 3 displays the main power board circuit along with the connections made for the SAS system, followed by the SAS topology shown in Figure 4.

B. PV Modeling and Implementation

The electrical characterization of PV generators typically focuses on analyzing the current-voltage and power-voltage

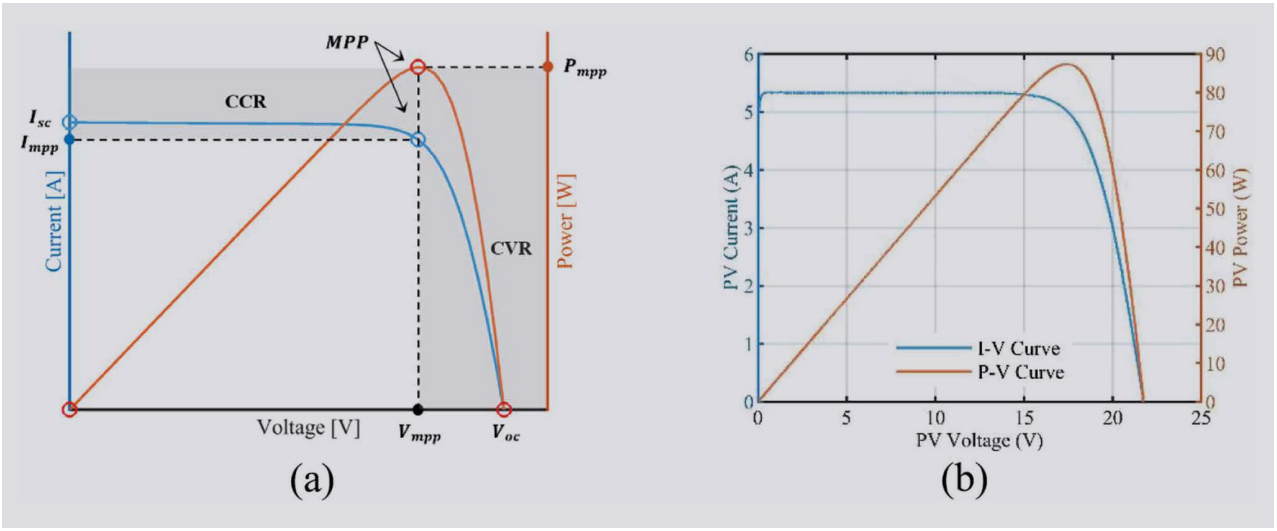

FIG 5 I-V and P-V curves. (a) Ideal curves. (b) SAS experimental curves.

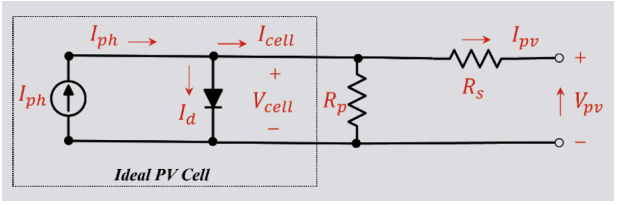

FIG 6 Single-diode model of a PV cell.

relationships, as depicted by their respective curves. Figure 5 illustrates these relationships, featuring ideal curves in Figure 5(a) and experimental curves derived using the developed SAS for a Kyocera KC85T PV panel in Figure 5(b). These curves highlight key parameters such as short circuit current (I_{sc}), open circuit voltage (V_{oc}), maximum power point (MPP), and the respective current, voltage, and power values at MPP (I_{mpp}, V_{mpp}, P_{mpp}). When analyzing solar simulators, two critical regions are identified: the constant current region (CCR) to the left of the MPP and the constant voltage region (CVR) to the right. In the CCR, minor changes in the current can significantly affect the voltage, whereas in the CVR, small voltage variations can lead to substantial current changes [9]. A PV electrical circuit model is derived to generate these nonlinear I-V characteristic curves.

An ideal PV cell is typically modeled as a current source parallel to a diode, known as the single-diode model. Figure 6 illustrates the model of practical PV cells, highlighting the parasitic resistances to account for device losses. The single-diode model is widely used for PV cells due to its balance between simplicity and accuracy [10].

The circuit diagram for the ideal PV cell shows that the current I_{ph} supplied by the source represents the current generated by the photon-electron interaction resulting from the absorption of solar radiation. Some of this current flows through the diode (I_d), while the remaining current flows out of the PV cell (I_{cell}). The equation for the current leaving the ideal PV cell can be written as:

$$I_{cell} = I_{ph} - I_d. \tag{1}$$

The general equation for the diode current can be further defined and plugged into Equation (1) as:

$$I_{cell} = I_{ph} - I_0\left[\exp\left(\frac{qV_{cell}}{akT_n}\right) - 1\right], \tag{2}$$

where I_0 is the dark/reverse saturation current of the diode [7]. The constant q represents the charge of an electron ($1.6022{\cdot}10^{-19}$ C), V_{cell} is the ideal cell voltage across the diode, a is the diode ideality constant, and k is the Boltzmann constant ($1.3807{\cdot}10^{-23}$ J/K). The nominal temperature T_n is typically considered to be 25 °C or $298.15^{\circ}K$ under standard testing conditions (STC). Equation (1) represents the ideal model for a single PV cell, but it does not take into account losses in the system, therefore series and parallel resistances (R_s, R_p) are added to account for these losses, leading to I_{pv} as:

$$I_{pv} = I_{ph} - I_0\left[\exp\left(\frac{V_{pv} + R_s I_{pv}}{V_t a}\right) - 1\right] - \frac{V_{pv} + R_s I_{pv}}{R_p}, \tag{3}$$

and I_0 is defined as:

$$I_0 = \frac{I_{sc,n} + K_I \Delta T}{\exp\left(\left(V_{oc,n} + K_V \Delta T\right)/(aV_t)\right) - 1}, \tag{4}$$

with $V_t = \frac{N_s kT}{q}$, N_s being the number of cells connected in series, $V_{oc,n}$ being the STC open-circuit voltage and K_V being the voltage temperature coefficient. Equation (3) is used to calculate the I-V characteristics of practical PV modules, which is integrated into the DSP of the Kit. Utilizing the parameter extraction methods and simplifications for R_s, R_p, a, I_{ph}, and I_0, as outlined in [10], I_{ph} is defined as:

$$I_{ph} = \left(I_{ph,n} + K_I \Delta T\right)\frac{G}{G_n}, \tag{5}$$

with K_I being the current temperature coefficients, $\Delta T = T - T_n$ being the difference between actual and STC temperature, and G and G_n being actual and STC irradiances, respectively. Furthermore, if the array is composed of a number of parallel connections (N_p), I_{ph} and I_0 can be multiplied by N_p each. The single-diode model is fully implemented for this simulator, yet it is noteworthy that students can easily implement more complex models, such as the double-diode model [5], to achieve higher accuracy in conditions like low irradiance or partial shading.

C. Design and Control of the Rectifier

A single-phase rectifier is used to convert ac electricity from the utility grid into the input side of the dc–dc buck converter. In this way, a dc power supply is no longer required. A θ-converter [11] is adopted for the rectifier. It consists of two legs: a conversion leg and a neutral leg. As shown in Figure 4, the conversion leg consists of switches Q_5 and Q_6, inductor L_3, and dc-bus capacitor C_{77}. The neutral leg consists of switches Q_3 and Q_4, inductor L_2, and capacitor C_{76}. The conversion leg is mainly used to control the grid current i_g to achieve unity power factor and acts as a half-bridge rectifier to regulate dc bus voltage V_{dc}. The neutral leg is responsible for regulating the output voltage V_+ and diverting ripples away from the output capacitor which becomes the input to the buck converter [11]. These two legs can be controlled independently, providing high flexibility for the controller. A self-synchronized universal droop control (SUDC) [12] is implemented for the control of the conversion leg and a proportional-integral (PI) control along with a resonant term is used to control the neutral leg.

D. Design and Control of the dc–dc Buck Converter

1) Electrical Design: The Kit is equipped with a set of built-in capacitors and inductors with the option for reconfiguration to implement the desired topology. It includes three capacitors (C_{79}, C_{78}, C_{80}), each with a capacitance of $20\ \mu F$, and two capacitors (C_{76}, C_{77}) with a capacitance of $470\ \mu F$ each. Similarly, there are three inductors (L_1, L_2, L_3), rated at $2\ \text{m}H$. For the buck converter's electrical components, the inductor L_1 and capacitor C_{79} on the output side, as shown in Figure 4, are deemed sufficient. This assessment is based on the application of standard design principles:

$$\Delta I_{\text{pp}} = \frac{V_{\text{in}}}{4 f_{\text{sw}} L_1}, \tag{6}$$

$$\Delta V_{\text{pp}} = \frac{\Delta I_{\text{pp}}}{8 f_{\text{sw}} C_{79}}, \tag{7}$$

with the Kit's switching frequency (f_{sw}) set at $20\ kHz$ and $V_{\text{in}} = V_+$ set at 200 V, this leads to maximum peak-to-peak values for current (ΔI_{pp}) and voltage (ΔV_{pp}) as 1.25 A and 0.39 V, respectively. These values are acceptable for this application.

2) Controller Design: Equation (3) is implemented with a set of low-pass filters (LPF) and resonant filters (K_R) shown in Figure 7 to generate a stable reference signal for the PCS to follow. The LPFs are designed with a cutoff frequency of 10 Hz and discretized according to the Kit's operational frequency (6.67 kHz) to reduce sensor noise. The resonant filter in the form of

$$K_R(s) = \frac{K_h 2\zeta h\omega s}{s^2 + 2\zeta h\omega s + (h\omega)^2}, \tag{8}$$

with $\zeta = 0.01$, $h = 1$, and $\omega = 2\pi f$, is implemented to reduce the fundamental component (60 Hz) in the output current and voltage of the SAS. The control of the dc–dc buck converter involves measuring the output current I_{pv} and comparing it with the reference current I_{ref} generated by the PV model, through a proportional-integral (PI) controller. The output of the controller u_b is then converted into PWM signals to drive the switches Q_1, Q_2 of the buck converter. The resonant term reduces the oscillations caused by the fundamental component from the grid in the output voltage. In this way, the steady state performance is improved. The parameters of the PI controller can be selected following classical design methods and the guidelines in [13] with the following relationship between the PI gains and output capacitance C_+:

$$K_p^2 = 2C_+ K_i, \tag{9}$$

where the relationship of K_p and K_i is mostly related to the capacitance C_+ at the output side of the rectifier and can be initially chosen to be small and gradually increased to achieve the desired performance. While this work employs a PI controller with a resonant term, other advanced control strategies can be implemented to further enhance the system's performance.

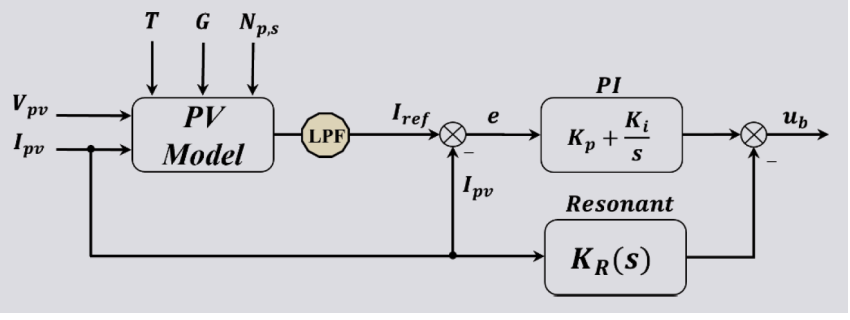

FIG 7 Controller for the SAS dc–dc buck converter.

E. HMI

The user interface is configured to send and receive data at a sampling rate of 10 ms and allows users to adjust *PV* parameters as shown in Figure 8. This flexibility is achievable because the PV model is digitally built-in using direct calculations derived from Equation (3), which is a function of G, T, N_s, N_p. The user can monitor signals such as reference current

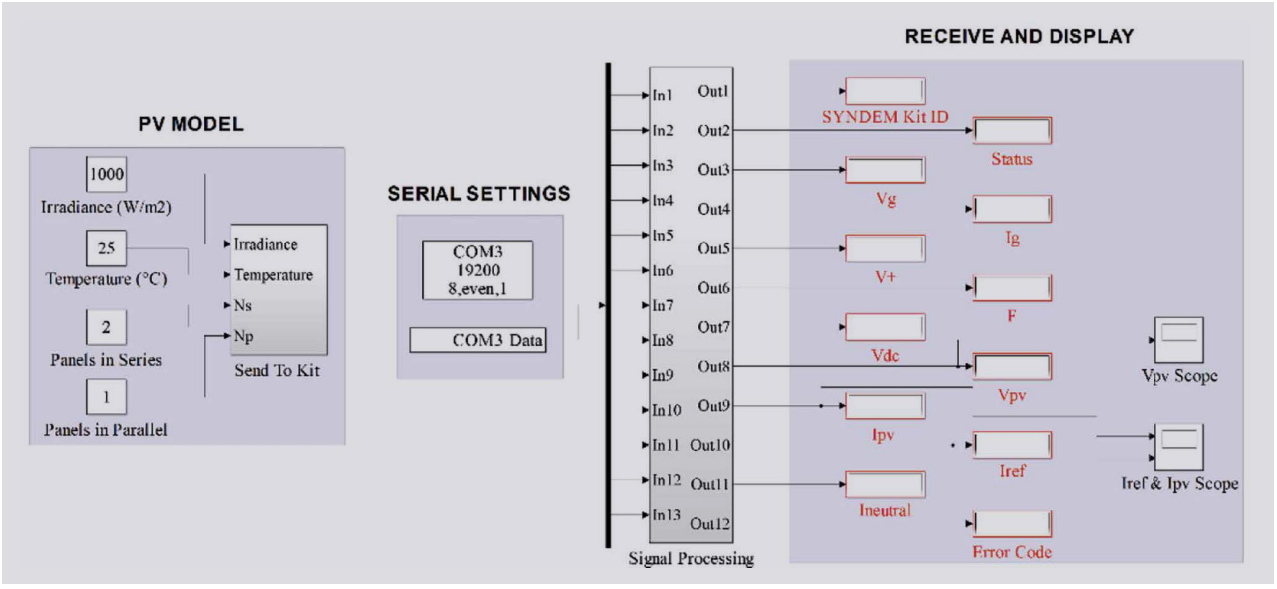

FIG 8 HMI in MATLAB/Simulink.

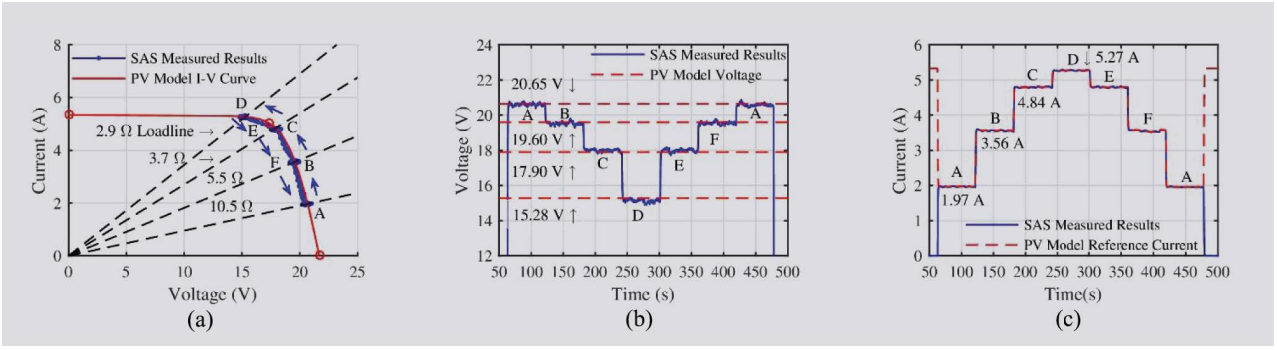

FIG 9 SAS results for KC85T module with multiple load changes. (a) SAS measured results on *I–V* curve. (b) Output voltage results. (c) Output current results.

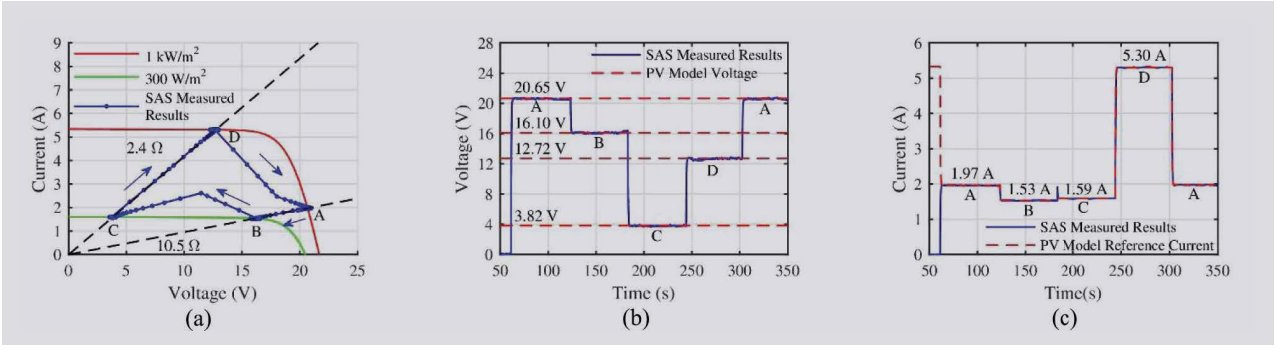

FIG 10 SAS results for irradiance change (A to B), load change (B to C), irradiance change (C to D), and load change (D to A). (a) SAS measured results on *I–V* curve. (b) Output voltage results. (c) Output current results.

produced by the PV model, output voltage, and output current. These signals can be conveniently analyzed and post-processed.

Experimental Results and Discussions

To validate the performance of the SAS, a Kyocera KC85T PV model is used as an example, with its parameters available in [14]. The assessment of the system's performance includes testing under varying load and irradiance conditions.

A. Load Change

An experimental test was conducted using four loads: 10.5 Ω, 5.5 Ω, 3.7 Ω, and 2.9 Ω. Figure 9(a) displays the measured operating points in the I–V curve when subjected to

step changes in loads. The system begins at point "A" located on the 10.5 Ω load line and cycles back after passing through the 5.5 Ω, 3.7 Ω, and 2.9 Ω loads. The intersection between the loads and the I-V curve determines the optimal operational voltage and current that the SAS must track. In this test scenario, operation point "A" has an ideal voltage and current setpoints of 20.65 V and 1.97 A, respectively. Point "B" and "F" have setpoints of 19.60 V and 3.56 A. Point "C" and "E" operates at 17.90 V and 4.84 A. And point "D," located left to the MPP has values of 15.28 V and 5.27 A. Figure 9(b) and (c) show the voltage and current tracking performance of the system, respectively.

To achieve realistic outdoor testing of PV systems, it is essential to be able to simulate changes in irradiance and temperature.

B. Irradiance Change

To achieve realistic outdoor testing of PV systems, it is essential to be able to simulate changes in irradiance and temperature. In Figure 10(a), the experimental results on the I-V curve are presented for both 1 kW/m^2 and 300 W/m^2 irradiance curves operating at two different load lines. The experimental test involved starting at point "A" with the 10.5 Ω load, shifting towards point "B," which represents a step down in irradiance. The load was then changed to 2.4 Ω resulting in the operating point "C," followed by a shift back up to the 1 kW/m^2 irradiance curve at point "D." Finally, the test cycled back to point "A" for a load change. In this test scenario, an aggressive change in irradiance was simulated by going from 1 kW/m^2 to 300 W/m^2 in the step-down and from 300 W/m^2 to 1 kW/m^2 in the step-up. Figure 10(b) and (c) illustrate the system's fast and accurate response to changes in the output voltage and current values, respectively, according to the PV model's reference.

Conclusion

The concept of "learning-by-doing" cultivates deep-thinking skills, preparing the next generation of engineers with hands-on skills essential for success in the rapidly growing renewable energy and power systems sector. This article exemplifies how learning-by-doing can be achieved through the Kit bridging the gap from theoretical design to experimental practice, using the design and implementation of a SAS as a practical demonstration. This approach allows researchers, educators, and students in power electronics and control to gain practical experience, allowing for straightforward modifications and a deeper understanding of electrical topologies, control algorithms, communication interfaces, data processing, and more.

Acknowledgment

This work was supported in part by the National Science Foundation under Grant #2328248.

About the Authors

Kevin Norman (kevin.b.norman@ttu.edu) is currently pursuing the Ph.D. degree with the Department of Mechanical Engineering, Texas Tech University, Lubbock, TX, USA. His current research interests include power electronics control applied to solar systems and smart microgrids.

Beibei Ren (beibei.ren@ttu.edu) is currently an Associate Professor of mechanical engineering and the Larry and Nancy McVay Endowed Professor in engineering with Texas Tech University, Lubbock, TX, USA. Her research focuses on control, microgrids, smart grid, and power electronics.

Qing-Chang Zhong (zhongqc@ieee.org) holds the Max McGraw Endowed Chair Professor in energy and power engineering with the Department of Electrical and Computer Engineering, Illinois Institute of Technology. He is also the Founder and the CEO of Syndem LLC, Chicago, USA. He currently chairs the Working Group of IEEE Standard on Virtual Synchronous Machines.

References

[1] Q.-C. Zhong et al., "Go real: Power electronics from simulations to experiments in hours: Versatile experimental tool for next generation engineers," *IEEE Power Electron. Mag.*, vol. 7, no. 3, pp. 52–61, Sep. 2020.

[2] Z. Zhang, C. T. Hansen, and M. A. E. Andersen, "Teaching power electronics with a design-oriented, project-based learning method at the technical university of Denmark," *IEEE Trans. Educ.*, vol. 59, no. 1, pp. 32–38, Feb. 2016.

[3] F. Martinez, L. C. Herrero, and S. de Pablo, "Project-based learning and rubrics in the teaching of power supplies and photovoltaic electricity," *IEEE Trans. Educ.*, vol. 54, no. 1, pp. 87–96, Feb. 2011.

[4] U. K. Shinde et al., "Solar PV emulator for realizing PV characteristics under rapidly varying environmental conditions," in *Proc. IEEE Int. Conf. Power Electron., Drives Energy Syst. (PEDES)*, Dec. 2016, pp. 1–5.

[5] R. Ayop and C. W. Tan, "A comprehensive review on photovoltaic emulator," *Renew. Sustain. Energy Rev.*, vol. 80, pp. 430–452, Dec. 2017.

[6] J. P. Ram et al., "Analysis on solar PV emulators: A review," *Renew. Sustain. Energy Rev.*, vol. 81, pp. 149–160, Jan. 2018.

[7] K. Nguyen-Duy, A. Knott, and M. A. E. Andersen, "High dynamic performance nonlinear source emulator," *IEEE Trans. Power Electron.*, vol. 31, no. 3, pp. 2562–2574, Mar. 2016.

[8] C. Ottieri, K. Ojiako, and S. M. S. Alarefi, "Simulink simulation of a current mode control DC-DC based PV emulator : Sustainable application of power electroincs in solar PV eduaction," in *Proc. Int. Symp. Power Electron., Electr. Drives, Autom. Motion (SPEEDAM)*, Jun. 2020, pp. 865–870.

[9] I. D. G. Jayawardana et al., "A fast-dynamic control scheme for a Power-Electronics-Based PV emulator," *IEEE J. Photovolt.*, vol. 11, no. 2, pp. 485–495, Mar. 2021.

[10] M. G. Villalva, J. R. Gazoli, and E. R. Filho, "Comprehensive approach to modeling and simulation of photovoltaic arrays," *IEEE Trans. Power Electron.*, vol. 24, no. 5, pp. 1198–1208, May 2009.

[11] Q.-C. Zhong and W.-L. Ming, "A θ-converter that reduces common mode currents, output voltage ripples, and total capacitance required," *IEEE Trans. Power Electron.*, vol. 31, no. 12, pp. 8435–8447, Dec. 2016.

[12] Q.-C. Zhong, W.-L. Ming, and Y. Zeng, "Self-synchronized universal droop controller," *IEEE Access*, vol. 4, pp. 7145–7153, 2016.

[13] W.-L. Ming, Q.-C. Zhong, and X. Zhang, "A single-phase four-switch rectifier with significantly reduced capacitance," *IEEE Trans. Power Electron.*, vol. 31, no. 2, pp. 1618–1632, Feb. 2016.

[14] *Kyocera KC85 Solar Panel | KC 85-Watt Solar Module*. Accessed: Jan. 22, 2024. [Online]. Available: https://www.solarelectricsupply.com/kyocera-85-watt-solar-panel-kc85

PEM